

Optimal weights for measuring redshift space distortions in multitracer galaxy catalogues

David W. Pearson,¹★ Lado Samushia^{1,2,3} and Praful Gagrani¹

¹*Department of Physics, Kansas State University, 116 Cardwell Hall, Manhattan, KS, 66506, USA*

²*National Abastumani Astrophysical Observatory, Ilia State University, 2A Kazbegi Ave., GE-1060 Tbilisi, Georgia*

³*Institute of Cosmology and Gravitation, University of Portsmouth, PO1 3FX, UK*

Accepted 2016 August 25. Received 2016 August 24; in original form 2016 June 10

ABSTRACT

Since the volume accessible to galaxy surveys is fundamentally limited, it is extremely important to analyse available data in the most optimal fashion. One way of enhancing the cosmological information extracted from the clustering of galaxies is by weighting the galaxy field. The most widely used weighting schemes assign weights to galaxies based on the average local density in the region (FKP weights) and their bias with respect to the dark matter field (PVP weights). They are designed to minimize the fractional variance of the galaxy power-spectrum. We demonstrate that the currently used bias dependent weighting scheme can be further optimized for specific cosmological parameters. We develop a procedure for computing the optimal weights and test them against mock catalogues for which the values of all fitting parameters, as well as the input power-spectrum are known. We show that by applying these weights to the joint power-spectrum of emission line galaxies and luminous red galaxies from the Dark Energy Spectroscopic Instrument survey, the variance in the measured growth rate parameter can be reduced by as much as 36 per cent.

Key words: methods: data analysis – galaxies: statistics – cosmological parameters – large-scale structure of Universe.

1 INTRODUCTION

Future galaxy redshift surveys, such as the Dark Energy Spectroscopic Instrument survey (DESI; Schlegel et al. 2011; Levi et al. 2013), the Extended Baryon Oscillation Spectroscopic survey (eBOSS; Schlegel et al. 2009), the *Euclid* satellite surveys (Laureijs et al. 2011), and the Wide Field Infrared Survey Telescope surveys (Spergel et al. 2013) will cover vast cosmological volumes with a high number density of galaxies. Since the available cosmic volume is fundamentally limited, a lot of effort is going into developing optimal ways of analysing galaxy clustering data (see e.g. Eisenstein et al. 2007; Blazek et al. 2014; Bianchi et al. 2015; Scoccimarro 2015; Slepian & Eisenstein 2016).

One way of improving the variance of measured 2-point statistics is to weight the galaxy field to achieve the optimal signal to noise. The most commonly used weighting scheme is the one developed by Feldman, Kaiser & Peacock (1994, hereafter FKP), which is used in all analyses employing 2-point statistics (see e.g. Percival et al. 2001; Reid et al. 2010; Beutler et al. 2011, 2012, 2014; Blake

et al. 2011; Anderson et al. 2012; Ross et al. 2013; Gil-Marín et al. 2015). The FKP weights,

$$w_{\text{FKP}}(\mathbf{r}) \propto \frac{1}{1 + \bar{n}(\mathbf{r})P(\mathbf{k})}, \quad (1)$$

where $\bar{n}(\mathbf{r})$ is the average number density of galaxies at a position \mathbf{r} and $P(\mathbf{k})$ is the power-spectrum at a wavelength of interest \mathbf{k} , are straightforward to apply and reduce the variance of the measured power-spectrum when the completeness of the galaxy sample is significantly non-uniform.

Percival, Verde & Peacock (2004, hereafter PVP) further optimized the FKP scheme for samples that include galaxies with a range of biases with respect to the dark matter. If the number density is uniform, the PVP weights are

$$w_{\text{PVP}} \propto b, \quad (2)$$

where b is the bias with respect to the dark matter, and will minimize the fractional variance in the measured power-spectrum.

If a galaxy sample covers such a wide redshift range that the effects of cosmic evolution are significant, the measured power-spectrum will be a weighted average of power spectra at different redshifts within that range. Since the sensitivity of the power-spectrum to cosmological parameters also varies with redshift, it is possible to construct redshift-dependent weights which

* E-mail: dpearson@phys.ksu.edu

maximize the constraining power of the measured power-spectrum for specific cosmological parameters. This optimal weighting scheme obviously depends on which cosmological parameters we want to optimize. Recently, Zhu, Padmanabhan & White (2015) derived redshift weights that optimize the measurement of the baryon acoustic oscillation (BAO) peak position, while Ruggeri et al. (2016) derived similar weights that optimize the redshift space distortion (RSD) parameter. Both works built on the formalism developed in Tegmark, Taylor & Heavens (1997).

Future surveys will observe emission line galaxies (ELGs), luminous red galaxies (LRGs), and quasars (QSOs), in overlapping volumes. Computing power spectra of all tracers individually is sub-optimal as important information encoded in the cross-correlation of the tracers will be lost. A promising way of taking advantage of the presence of multiple tracers was proposed in McDonald & Seljak (2009). The method, however, has not yet been implemented in practice and will only result in a significant improvement in constraining power when the number density of tracers is high (which is not the case, e.g. in the eBOSS survey). Computing all auto and cross-power spectra is possible (Ross et al. 2012) but will require accurate estimation of large covariance matrices which may be problematic for future surveys (Pope & Szapudi 2008; Schneider et al. 2011; de Putter et al. 2012; Xu et al. 2012; de la Torre et al. 2013; Mohammed & Seljak 2014; Paz & Sanchez 2015; Grieb et al. 2016; Pearson & Samushia 2016). The most straightforward way is to compute a single power-spectrum for all tracers while differentially weighting them to achieve optimal signal to noise by applying the PVP weights.

While the PVP weights are designed to minimize the fractional variance in the power-spectrum, this does not necessarily translate into minimal variance on measured cosmological parameters. A good example of this is the growth rate parameter, f .¹ The growth rate is measured from an anisotropic signature in the power-spectrum which is more pronounced for low-biased tracers. The power-spectrum signal, on the other hand, is stronger in the high-biased tracers. The weights in equation (2) upweight high-bias galaxies to achieve the optimal power-spectrum signal, but the measured power-spectrum becomes less sensitive to f . The optimal weighting for the growth rate parameter must counterbalance these two tendencies by producing a power-spectrum with a small (not necessarily minimal) variance that is, at the same time, sensitive enough to the f parameter.

In this work, we generalize the PVP weighting scheme to minimize the variance of specific cosmological parameters measured from the power-spectrum (Section 2). We assume that the galaxy samples will be analysed in narrow redshift bins of $\delta z \sim 0.1$, eliminating the need to consider the redshift evolution weights (Zhu et al. 2015; Ruggeri et al. 2016) as the effect will be small. We test our new weighting scheme on mock catalogues of the eBOSS and DESI surveys (Section 3) and show that they could improve the variance of the measured f parameter by up to 36 per cent. As expected, the optimal weights differ for different cosmological parameters (Section 4). This weighting scheme is straightforward to compute and implement and should result in reduced variance on cosmological parameters measured from future galaxy surveys (Section 5).

2 OPTIMAL WEIGHTING

For simplicity, we will assume that the galaxies of two types with densities $n_1(\mathbf{r})$ and $n_2(\mathbf{r})$ are present in an overlapping volume and the average number densities, \bar{n}_1 and \bar{n}_2 , do not vary significantly within the volume. The formalism is easy to generalize for more than two tracers and varying number densities. If we assign weights w_1 and w_2 to these galaxies, then the number density of the combined field is

$$n(\mathbf{r}) = w_1 n_1(\mathbf{r}) + w_2 n_2(\mathbf{r}) \quad (3)$$

and the overdensity field is

$$\delta(\mathbf{r}) \equiv \frac{n(\mathbf{r}) - \bar{n}}{\bar{n}} = A_1 \delta_1(\mathbf{r}) + A_2 \delta_2(\mathbf{r}), \quad (4)$$

where the overdensities are defined by

$$\delta_i(\mathbf{r}) = \frac{n_i(\mathbf{r}) - \bar{n}_i}{\bar{n}_i}, \quad (5)$$

and

$$A_i = \frac{w_i \bar{n}_i}{w_1 \bar{n}_1 + w_2 \bar{n}_2} \quad (6)$$

is the weighted fractional density. We will assume the weights to be normalized by $w_1 + w_2 = 1$. This will shorten some of our formulas, although, in practice, only the ratio of weights is relevant. The power-spectrum of the overdensity field,

$$P(\mathbf{k}) \equiv \left| \tilde{\delta}(\mathbf{k}) \right|^2, \quad (7)$$

can be estimated from the squared modulus of the Fourier transform,

$$\tilde{\delta}(\mathbf{k}) = \int d\mathbf{r} e^{-i\mathbf{k}\cdot\mathbf{r}} \delta(\mathbf{r}), \quad (8)$$

We will assume that the overdensity fields are Gaussian (this is a common assumption when deriving optimal weights) with

$$\langle \tilde{\delta}_i(\mathbf{k}) \tilde{\delta}_j^*(\mathbf{k}) \rangle = \left[(b_i + \mu^2 f) (b_j + \mu^2 f) P_m(k) + \frac{\delta_{ij}^c}{\bar{n}_i} \right] V_s, \quad (9)$$

where the angular brackets denote the expectation value, δ^c is a Kronecker delta function, V_s is the survey volume, and $P_m(k)$ is the matter power-spectrum that can be computed in any given cosmological model (Kaiser 1987; Hamilton 1997). The last term in equation (9) is the shot-noise term due to the sampling of the overdensity field with a finite number of galaxies (FKP).² For the weighted field in equation (4), this results in

$$P(\mathbf{k}) = \left[(b_{\text{eff}}^{w_1 w_2} + \mu^2 f)^2 P_m(k) + S^{w_1 w_2} \right] V_s, \quad (10)$$

with the weighting dependent effective bias,

$$b_{\text{eff}}^{w_1 w_2} = A_1 b_1 + A_2 b_2, \quad (11)$$

and the shot-noise term,

$$S^{w_1 w_2} = \frac{A_1^2}{\bar{n}_1} + \frac{A_2^2}{\bar{n}_2}. \quad (12)$$

Since we assumed the overdensity field to be Gaussian, the variance of the galaxy power-spectrum estimator is simple to compute and is

$$\text{Var}[P(\mathbf{k})] \propto \left[(b_{\text{eff}}^{w_1 w_2} + \mu^2 f)^2 P_m(k) + S^{w_1 w_2} \right]^2 \quad (13)$$

¹ In practice, from the galaxy clustering data alone, the growth rate parameter is measured up to a normalization constant $f\sigma_8$. We will be using f to mean the $f\sigma_8$ combination for brevity. This has no effect on our results.

² The power-spectrum estimators are usually defined after subtracting the shot-noise term, but this is irrelevant for our results.

(FKP, PVP; Tegmark et al. 1997). The fractional variance in the galaxy power-spectrum is then

$$\frac{P(\mathbf{k})}{\text{Var}[P(\mathbf{k})]} \propto \frac{(b_{\text{eff}}^{w_1 w_2} + \mu^2 f)^2 P_m(k)}{\left[(b_{\text{eff}}^{w_1 w_2} + \mu^2 f)^2 P_m(k) + S^{w_1 w_2} \right]^2}. \quad (14)$$

This expression is minimized³ by

$$w_1 = \frac{b_1}{b_1 + b_2}, \quad (15)$$

$$w_2 = \frac{b_2}{b_1 + b_2},$$

which, for constant number densities, is equivalent to PVP weighting.⁴

The minimum fractional variance in the power-spectrum, however, does not necessarily correspond to the minimum variance in the cosmological parameters derived from the power-spectrum. The power-spectrum is most sensitive to the bias $-b_{\text{eff}}$, growth rate $-f$, and the Alcock–Paczynski parameters α_{\parallel} and α_{\perp} (Alcock & Paczynski 1979; Kaiser 1987). The dependence on b and f is already in equation (10), and the dependence on α_{\perp} and α_{\parallel} can be introduced by replacing

$$k \longrightarrow \frac{k}{\alpha_{\perp}} \left[1 + \mu^2 \left(\frac{\alpha_{\perp}^2}{\alpha_{\parallel}^2} - 1 \right) \right]^{1/2}, \quad (16)$$

$$\mu \longrightarrow \frac{\mu \alpha_{\perp}}{\alpha_{\parallel}} \left[1 + \mu^2 \left(\frac{\alpha_{\perp}^2}{\alpha_{\parallel}^2} - 1 \right) \right]^{-1/2}, \quad (17)$$

and dividing the power-spectrum by a factor of $\alpha_{\parallel} \alpha_{\perp}^2$ (Ballinger, Peacock & Heavens 1996; Simpson & Peacock 2010; Samushia et al. 2011). The Fisher information matrix of these parameters is

$$F_{ij} = \int d\mathbf{k} \frac{\partial P(\mathbf{k})}{\partial \theta_i} \frac{1}{\text{Var}[P(\mathbf{k})]} \frac{\partial P(\mathbf{k})}{\partial \theta_j}, \quad (18)$$

where $\theta = (b_{\text{eff}}, f, \alpha_{\parallel}, \alpha_{\perp})$ is a parameter vector, and the integration is over all wavevectors, the power-spectrum measurements of which were used in the analysis. The inverse of the Fisher matrix gives a covariance matrix

$$\mathbf{C} = \mathbf{F}^{-1}, \quad (19)$$

and the diagonal elements of the covariance matrix correspond to the expected variance of the parameters measured from the power-spectrum. Because of the presence of the derivative terms (that also depend on the weights) in equation (18), the weighting scheme that minimizes the variance of the power-spectrum does not necessarily minimize the diagonal elements of the covariance matrix in equation (19).

A simple analytic solution for the optimal weights in this case does not exist, but they are relatively straightforward to find numerically. To find the optimal weights, we numerically compute the variance and the derivatives in equation (18) and take the integral over the wavevectors of interest. We then numerically find the weights that minimize the diagonal elements of the inverse Fisher

matrix of equation (19).⁵ These weights will, in general, be different for each parameter. In the tradition of FKP and PVP, we refer to these as PSG weights in what follows.

3 DATA AND MEASUREMENT PROCEDURES

3.1 The sample

In order to test our weighting scheme, we generated lognormal mock catalogues (Coles & Jones 1991) giving us control over the input power-spectrum and linear growth rate.

We computed the matter power-spectrum using the CAMB software (Lewis, Challinor & Lasenby 2000) via the web interface hosted at Legacy Archive for Microwave Background Data Analysis (LAMBDA)⁶ for a spatially flat Λ cold dark matter cosmology with $\Omega_M = 0.276$, and $\Omega_b h^2 = 0.0226$. We use the fiducial value of

$$f(\Omega_M, z) \approx \Omega_M^{0.6}(z), \quad (20)$$

where

$$\Omega_M(z) = \frac{\Omega_{M,0}(1+z)^3}{\Omega_{M,0}(1+z)^3 + \Omega_{\Lambda,0}}, \quad (21)$$

which is the value predicted by general relativity (Peebles 1980; Martínez & Saar 2002).

Our lognormal code was largely based on the description given in Weinberg & Cole (1992) and appendix A of Beutler et al. (2011), with modifications required to obtain a distribution of two tracers cross-correlated by the same underlying matter field.

We started by distributing the power to two grids – one for LRGs and one for ELGs – in k -space as

$$P(\mathbf{k}) = (b_i + \mu^2 f)^2 P_m(k), \quad (22)$$

where $\mu = k_z/k$ and b_i is the bias of LRGs or ELGs for the redshift bin. This was assigned to the real part only, with the imaginary part being set to zero. After performing inverse Fourier transforms using the complex-to-real transform in the Fastest Fourier Transform in the West (FFTW) library⁷ (Frigo & Johnson 2005), we took the resulting correlation functions and calculated $\ln[1 + \xi^i(\mathbf{r})]$ at each grid point, then performed real-to-complex transforms. The result of these transforms, $P_{\text{LN}}^i(\mathbf{k})$, was then normalized by the number of grid points, since FFTW produces the unnormalized Fourier transform.

At this stage, we took the ratio of the $P_{\text{LN}}^i(\mathbf{k})$ at each grid point in k -space and stored that in memory. We then constructed Gaussian random realizations by drawing from a normal distribution, centred on zero, with $\sigma = \sqrt{\max\{0, \text{Re}[P_{\text{LN}}^i(\mathbf{k})]\}/2}$, at each grid point for both the real and imaginary parts, in order to obtain a well-behaved power-spectrum (Weinberg & Cole 1992). We took care that $\delta_{\text{LN}}(-\mathbf{k}) = \delta_{\text{LN}}^*(\mathbf{k})$, and that the values at grid points whose indices are combinations of zero and $N_i/2$, where N_i is the number of grid points in dimension i , were purely real. This ensured that when we inverse Fourier transformed $\delta_{\text{LN}}(\mathbf{k})$, the result was purely real. We only did the random draw for the higher bias tracer, then using the ratio previously calculated, we scaled the random realization to obtain the values on the grid for the lower bias tracer. In this way,

³ This can be verified by simply equating the partial derivatives of equation (14) with respect to the weights to zero along with the Legendre multipliers to enforce the condition $w_1 + w_2 = 1$.

⁴ For a more rigorous derivation also accounting for the number density variations, see PVP.

⁵ Since we adopt the normalization $w_1 + w_2 = 1$, this turns into a simple one-parameter minimization procedure.

⁶ http://lambda.gsfc.nasa.gov/toolbox/tb_camb_form.cfm

⁷ <http://fftw.org/>

Table 1. Mock catalogue properties. Column 1 list the redshift range. Columns 2–4 list the volume of the cube and the number densities for LRGs and ELGs to match the eBOSS survey, respectively. Columns 5–7 list the volume of the cube and the number densities for LRGs and ELGs to match that expected in the DESI survey, respectively. Columns 8 and 9 list the biases for the LRGs and ELGs, respectively. Lastly, column 7 lists the dimensionless linear growth rate for the redshift bin.

Redshift	V_{eBOSS} ($h^{-3} \text{ Gpc}^3$)	$\bar{n}_{\text{LRG,eBOSS}}$ ($10^{-4} h^3 \text{ Mpc}^{-3}$)	$\bar{n}_{\text{ELG,eBOSS}}$ ($10^{-4} h^3 \text{ Mpc}^{-3}$)	V_{DESI} ($h^{-3} \text{ Gpc}^3$)	$\bar{n}_{\text{LRG,DESI}}$ ($10^{-4} h^3 \text{ Mpc}^{-3}$)	$\bar{n}_{\text{ELG,DESI}}$ ($10^{-4} h^3 \text{ Mpc}^{-3}$)	b_{LRG}	b_{ELG}	f
$0.6 \leq z < 0.7$	0.272	0.772	1.345	2.538	4.589	1.704	2.339	1.376	0.759
$0.7 \leq z < 0.8$	0.325	0.642	2.051	3.031	4.555	10.482	2.450	1.441	0.787
$0.8 \leq z < 0.9$	0.374	0.330	1.559	3.491	2.655	7.711	2.563	1.508	0.812
$0.9 \leq z < 1.0$	0.419	0.091	0.586	3.914	0.973	7.490	2.678	1.575	0.834

we were able to effectively obtain mock samples with two tracers, each following the same underlying matter distribution.

The last step was then to take the inverse Fourier transforms of the random realization for the higher bias tracer, and the scaled realization for the lower bias tracer. This resulted in overdensity fields for both tracers, $\delta_i(\mathbf{r})$, having zero mean and variance σ_G^2 . From these overdensity fields, we calculated the lognormal density field

$$\delta_{\text{LN},i}(\mathbf{r}) = \exp[\delta_i(\mathbf{r}) - \sigma_G^2/2]. \quad (23)$$

This was then multiplied by the average number of galaxies per cell to give the desired number density, and Poisson sampled to create our final galaxy catalogues, placing the galaxies randomly within a given cell.

We generated 1024 mock catalogues for four redshift bins in $0.6 < z < 1.0$. They contained two tracers designed to mimic LRGs and ELGs. This led to a total of 4096 mock catalogues with number densities to match those expected in the eBOSS survey, and 4096 with number densities to match those expected in the DESI survey. Table 1 lists the specific properties for the mock catalogues. For the eBOSS mocks, the number densities were calculated from information in Zhao et al. (2016). The volumes were calculated for the 1500 deg^2 region where the ELGs and LRGs would overlap. The DESI number densities were calculated from information in the DESI Science Final Design Report (DESI Collaboration 2016), and the volumes assume the $14\,000 \text{ deg}^2$ baseline survey footprint. The biases for the different redshift bins were given by Dawson et al. (2016).

To have a clean separation between number density-dependent and bias-dependent weights, our mock catalogues have a constant number density. Since there are no number density gradients, the FKP weights reduce to a simple uniform weighting (see Section 4), meaning that any improvements are only coming from the differential weighting of tracers based on their bias.

3.2 Measuring the power-spectrum

We followed the general methods of FKP for measuring the power-spectrum from our mock catalogues. We generated random catalogues with 10 or 30 times the number of each tracer for the DESI and eBOSS mocks, respectively. The galaxies and randoms were binned using cloud-in-cell interpolation (Birdsall & Fuss 1969) with one of the three different weighting schemes – see Section 4 for details. Since we used a discrete Fourier transform of boxes with a finite linear size $L = V^{1/3}$ (see Table 1 for volumes), our $\tilde{\delta}(\mathbf{k})$ (and correspondingly $P(\mathbf{k})$ measurements) were given on a discrete cubic grid with a resolution of $2\pi/L$. To compress this information, we computed the spherically averaged power-spectrum monopole

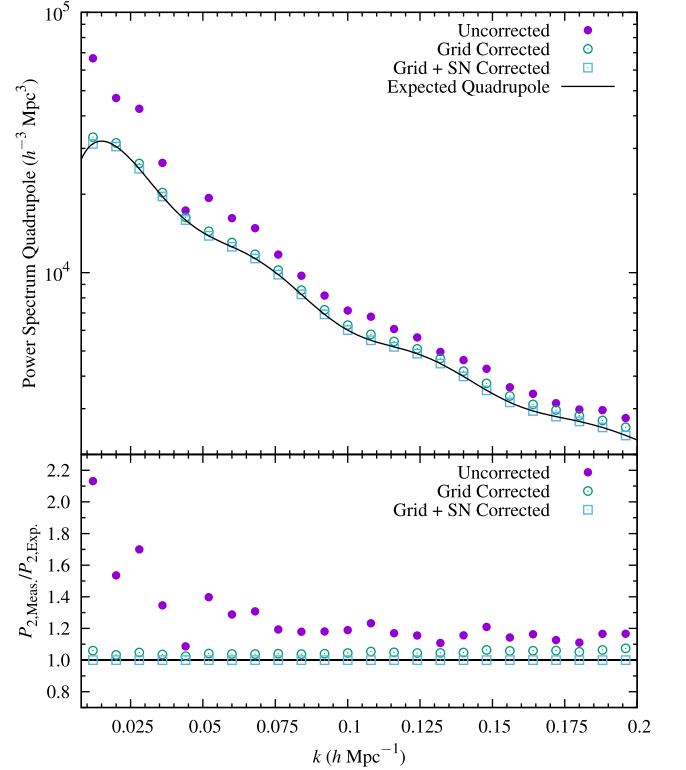


Figure 1. Here we show the effects of the discreteness of the grid on the quadrupole for the number densities and volume of the first redshift bin of eBOSS. The solid circles (purple) show the model power after being distributed to the grid, binned as in equation (24) and adding the expected shot noise calculated as in equation (26). The open circles (green) show the effects of the correction in equation (28). It is clear that even after applying that correction, there is a small positive bias (~ 5 per cent). The open squares (light blue) show the measured quadrupole after correcting for the discreteness in the shot noise as well, at which point we have recovered the expected quadrupole quite well.

and quadrupole ($l = 0, 2$) in 24 bins of width $\Delta k = 0.008$ for $0.008 \leq k \leq 0.2$ via

$$P_l(k) = \frac{2l+1}{2} \sum |\tilde{\delta}(\mathbf{k})|^2 \mathcal{P}_l[\mu(\mathbf{k})] G^2(\mathbf{k}), \quad (24)$$

where the sum is over all wavevectors in the range $k - \Delta k/2 \leq |\mathbf{k}| < k + \Delta k/2$, $\mathcal{P}_l(x)$ are the Legendre polynomials, and $G(\mathbf{k})$ is a grid correction term

$$G(\mathbf{k}) = \prod_i [\text{sinc}(\Delta L_i k_i)]^{-2}, \quad (25)$$

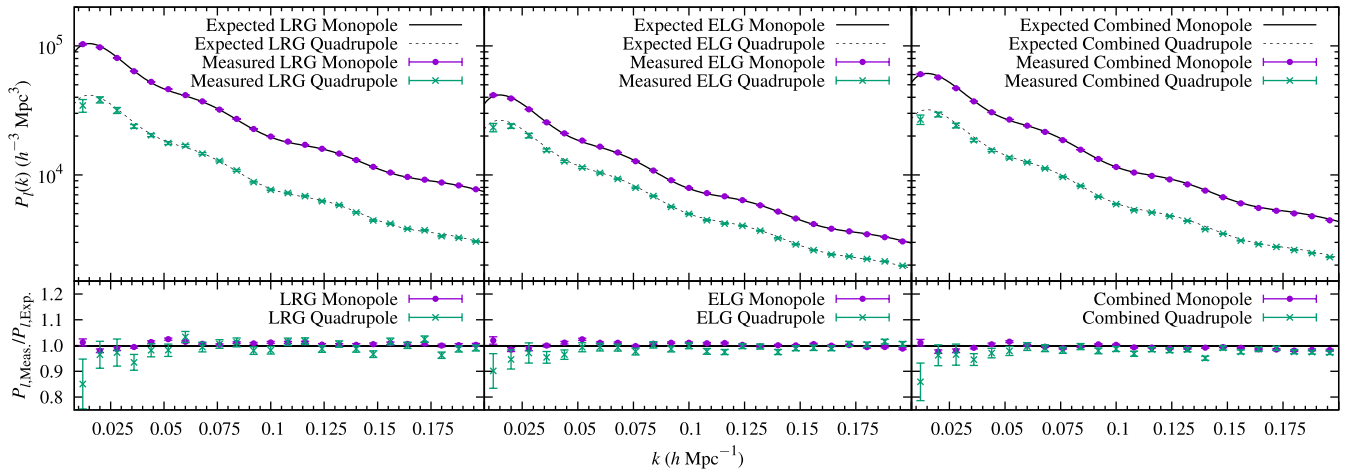


Figure 2. Comparison of the expected power-spectrum monopole and quadrupole with the measured values after applying all corrections for LRGs (left), ELGs (middle) and the combined sample (right) with equal weighting in the first redshift bin with eBOSS number densities. The plotted error bars are $\sqrt{C_{ii}/N}$, where C_{ii} are the diagonal elements of the sample covariance matrix, and N is the number of mocks.

Table 2. The PSG weights for the free parameters in our model. Column 1 indicates the target survey for the weights. Column 2 gives the redshift range. Columns 3–6 give the optimal weights for each parameter individually.

Survey	Redshift range	b	f	α_{\perp}	α_{\parallel}
DESI	$0.6 \leq z < 0.7$	(0.279, 0.721)	(0.207, 0.793)	(0.546, 0.454)	(0.464, 0.536)
	$0.7 \leq z < 0.8$	(0, 1)	(0, 1)	(0.516, 0.484)	(0.347, 0.653)
	$0.8 \leq z < 0.9$	(0, 1)	(0, 1)	(0.547, 0.453)	(0.429, 0.571)
	$0.9 \leq z < 1.0$	(0, 1)	(0, 1)	(0.568, 0.432)	(0.472, 0.528)
eBOSS	$0.6 \leq z < 0.7$	(0.427, 0.573)	(0.367, 0.633)	(0.589, 0.411)	(0.547, 0.453)
	$0.7 \leq z < 0.8$	(0.405, 0.595)	(0.326, 0.674)	(0.589, 0.411)	(0.544, 0.456)
	$0.8 \leq z < 0.9$	(0.447, 0.553)	(0.385, 0.615)	(0.597, 0.403)	(0.559, 0.441)
	$0.9 \leq z < 1.0$	(0.501, 0.499)	(0.471, 0.529)	(0.609, 0.391)	(0.580, 0.420)

with $\text{sinc}(x) = \sin(x)/x$, $\Delta L_i = L_i/N_i$, i denotes one of the three Cartesian coordinates, L_i is the length of the cube in that coordinate direction, and N_i is the corresponding number of grid points.

We only considered the power-spectrum measurements below $k \sim 0.2$ allowing us to safely ignore the non-linear effects at higher wavenumbers which are difficult to model and are usually excluded from the analysis. Even though our Fisher matrix predictions in Section 2 implicitly assumed that each $P(k)$ measurement would be analysed individually without reducing them to the multipoles, we do not expect this to be a big effect as a number of recent studies showed that reducing the power-spectrum to the first few even multipoles retains most of the information (Taruya, Saito & Nishimichi 2011; Kazin, Sánchez & Blanton 2012).

The measurements resulting from equation (24) were then corrected for shot noise

$$S_l(k) = \frac{1}{N_k} \left(\sum_{\text{gal}} w_i^2 + \alpha^2 \sum_{\text{ran}} w_i^2 \right) \sum_{\mu} \mathcal{P}_l(\mu), \quad (26)$$

where the sum is over the same modes, with $\alpha = \sum_{\text{gal}} w_i / \sum_{\text{ran}} w_i$, and then normalized by

$$I = V_s (\bar{n}_{\text{LRG}} w_{\text{LRG}} + \bar{n}_{\text{ELG}} w_{\text{ELG}})^2. \quad (27)$$

Since the power-spectrum multipoles in equation (24) were computed as a discrete sum over a finite number of wavenumbers, modelling them as angular integrals over the theoretical power-spectrum of equation (22) would be inaccurate. To model the k -grid discreteness effects, we distributed the model power to the same grid used to

calculate the power-spectrum from the mocks and binned it according to equation (24) to give $P_l^{\text{grid}}(k)$. We then adjusted the measured value,

$$P_l(k) \longrightarrow P_l(k) - \left[P_l^{\text{grid}}(k) - P_l^{\text{int}}(k) \right], \quad (28)$$

where

$$P_l^{\text{int}}(k) = \frac{2l+1}{2} \int_{-1}^1 (b_{\text{eff}}^{w_1 w_2} + \mu^2 f)^2 P_m(k) \mathcal{P}_l(\mu) d\mu, \quad (29)$$

is the integrated power-spectrum (Blake et al. 2011; Beutler et al. 2014). This effect (correction term in the brackets) is extremely small for the monopole, so, in practice, we only applied the correction to the quadrupole.

We would like to emphasize that, given the small volume of our mocks (especially the eBOSS mocks), the k -grid discreteness effects also had to be accounted for when computing the shot-noise correction. Even though integrals over higher order Legendre polynomials are zero, the discrete sum over μ in equation (26) is non-zero. This implies that the shot-noise corrections have to be applied not only to the monopole but to the higher order multipoles of the power-spectrum as well. Fig. 1 explicitly shows these effects on the quadrupole for the first redshift bin eBOSS mocks. We found that ignoring the effects in equation (28) can bias the quadrupole by ~ 27 per cent on average, and significantly more so at low wavenumbers. While significantly smaller, ignoring the discreteness effects in the shot noise – equation (26) – can bias the quadrupole by ~ 5 per cent. We note that the size of these

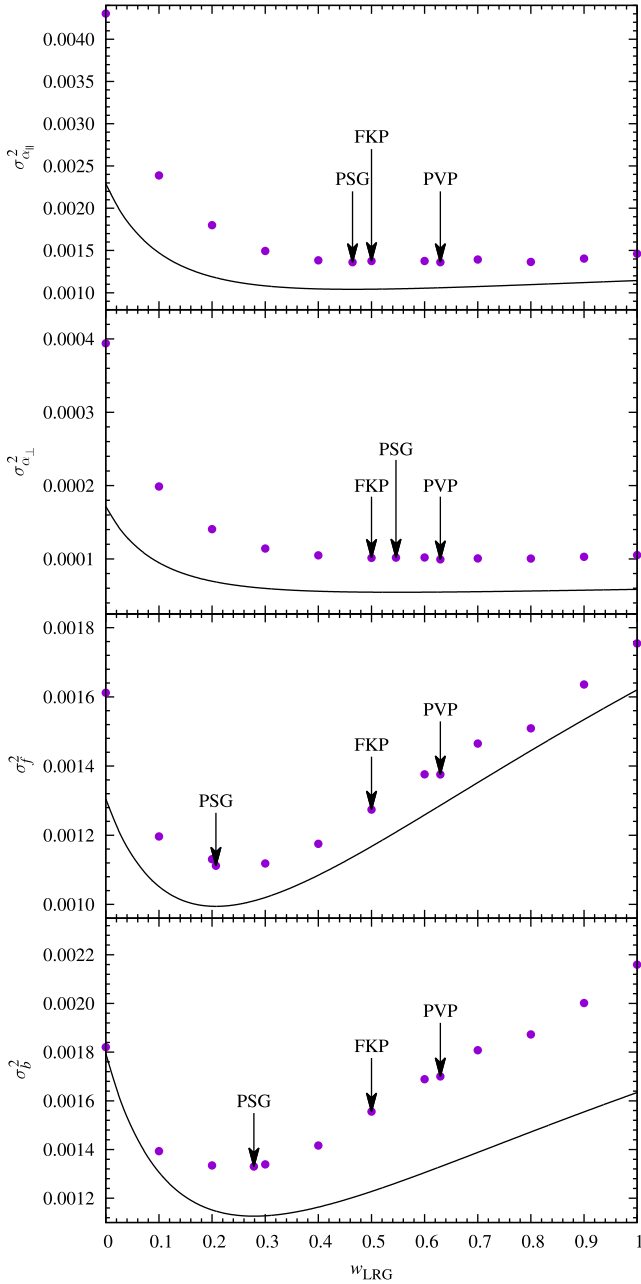


Figure 3. Variance of each parameter versus the relative weight of the LRGs for the first redshift bin of the DESI mocks. The points associated with the **FKP**, **PVP**, and **PSG** weights have been labelled. The solid lines are the theoretical predictions for the variance. In general, the points follow the shapes of the theoretical curves. For b and f , the **PSG** weights are clearly optimal, while for α_{\perp} and α_{\parallel} , the variance is flat for a broad range of weights leading all weighting schemes to perform equally well.

corrections decrease for increased volume, and the shot noise additionally decreases for increased number densities. For example, in the first redshift bin of the DESI mocks, the effect in equation (28) drops to ~ 13 per cent on average, while the shot noise causes a bias of less than 1 per cent.

Fig. 2 shows a detailed comparison of the power-spectrum which we expected to recover and the power-spectrum that we actually measured for the first redshift bin ($0.6 \leq z < 0.7$) with the eBOSS number densities and volume. We explicitly show the recovered power for each tracer individually as the confirmation of our scal-

ing procedure (see Section 3.1). We also note that we recovered the expected power-spectrum extremely well for the other eBOSS redshift bins and for the DESI volumes as well.

3.3 Parameter estimation

We model the measured power-spectrum multipoles as

$$P_l(k) = \frac{2l+1}{2\alpha_{\perp}^2\alpha_{\parallel}} \int_{-1}^1 d\mu P(k, \mu) P_l(\mu), \quad (30)$$

where

$$P(k, \mu) = (b_{\text{eff}}^{w_1 w_2} + \mu^2 f)^2 P_m(k), \quad (31)$$

and k , and μ depend on α_{\perp} and α_{\parallel} as in equations (16) and (17). The shape of the power-spectrum is fixed, while the four parameters $b_{\text{eff}}^{w_1 w_2}$, f , α_{\parallel} , α_{\perp} are free.⁸

In order to find the best-fitting parameters, we used a Markov Chain Monte Carlo (MCMC) method with the Metropolis–Hastings algorithm (Hastings 1970) to find the posterior likelihood of the free parameters. In all our MCMC chains, the mean values of the parameters were very close to the input values and the likelihood surfaces were close to Gaussian. We computed the variance of each parameter from the MCMC mocks and compared the resulting values for all the parameters for a specific set of weights to other weighting schemes to see if the **PSG** weights actually yield the tightest constraints.

4 COMPARISON WITH OTHER WEIGHTING SCHEMES

In order to test the weights purely from the stand point of relative weighting of tracers, our mock catalogues have uniform number densities throughout, and only two types of tracers with constant biases. In what follows, for brevity, we will quote weights as pairs in the form $(w_{\text{LRG}}, w_{\text{ELG}})$.

Because of the simplified nature of our mocks, the **FKP** weights are then simply (0.5, 0.5), regardless of the target survey or redshift bin. Similarly, the **PVP** weights will be the same, regardless of the target survey or redshift bin and will result in upweighting the LRGs as they have a higher bias – see equation (15). Since $b_{\text{LRG}} \simeq 1.7b_{\text{ELG}}$ at all redshifts (Dawson et al. 2016; Zhao et al. 2016), the **PVP** weights are (0.63, 0.37). The **PSG** weights vary from redshift bin to redshift bin somewhat, and from survey to survey, due to the varying relative number densities of the tracers. They are also different for different model parameters. We compute them following the numerical procedure outlined in Section 2.

Table 2 summarizes the **PSG** weights for the different redshift bins of the two surveys. In some cases, the **PSG** weights are close to the **FKP** or **PVP** weights, but in many cases, differ substantially. It is also interesting to note that for the DESI mocks, the **PSG** weights actually imply that above a redshift of 0.7, it would be better to consider only the ELGs when measuring the RSD parameters. However, this does not mean that the LRG and cross-power spectra do not contain additional information. The LRG, ELG and cross-power spectra (with appropriate covariance matrices) in principle contain all of the information. Our weighting in some sense gives the most optimal mixture (best principle component) of the three if they were to be reduced to a single power-spectrum, but other orthogonal mixtures (next principle components) will, of course,

⁸ Hereafter, we simply refer to $b_{\text{eff}}^{w_1 w_2}$ as b for simplicity.

Table 3. Comparison of **FKP** and **PVP** weights with those derived here (PSG). Column 1 indicates the target survey. Column 2 lists the redshift range. Column 3 indicates the weighting scheme. The remaining columns list the variance in each of the parameters.

Survey	Redshift range	Weights	σ_b^2	σ_f^2	$\sigma_{\alpha_{\perp}}^2$	$\sigma_{\alpha_{\parallel}}^2$
DESI	$0.6 \leq z < 0.7$	FKP	0.001 56	0.001 27	0.000 10	0.001 38
		PVP	0.001 70	0.001 38	0.000 10	0.001 36
		PSG	0.001 33	0.001 11	0.000 10	0.001 36
	$0.7 \leq z < 0.8$	FKP	0.000 78	0.000 64	0.000 07	0.000 94
		PVP	0.000 93	0.000 77	0.000 08	0.000 98
		PSG	0.000 56	0.000 49	0.000 07	0.000 97
	$0.8 \leq z < 0.9$	FKP	0.000 76	0.000 61	0.000 07	0.000 94
		PVP	0.000 85	0.000 67	0.000 07	0.000 90
		PSG	0.000 60	0.000 52	0.000 07	0.000 92
	$0.9 \leq z < 1.0$	FKP	0.000 60	0.000 55	0.000 07	0.000 84
		PVP	0.000 64	0.000 58	0.000 06	0.000 82
		PSG	0.000 57	0.000 53	0.000 07	0.000 85
eBOSS	$0.6 \leq z < 0.7$	FKP	0.035 99	0.027 75	0.003 43	0.055 80
		PVP	0.041 86	0.031 20	0.003 20	0.055 88
		PSG	0.035 46	0.027 09	0.003 05	0.052 59
	$0.7 \leq z < 0.8$	FKP	0.018 67	0.015 26	0.001 74	0.029 83
		PVP	0.021 00	0.016 86	0.001 68	0.028 89
		PSG	0.017 94	0.015 49	0.001 68	0.028 62
	$0.8 \leq z < 0.9$	FKP	0.023 81	0.020 65	0.002 57	0.039 18
		PVP	0.025 70	0.022 15	0.002 45	0.037 49
		PSG	0.024 86	0.022 13	0.002 42	0.039 17
	$0.9 \leq z < 1.0$	FKP	0.054 72	0.050 63	0.008 96	0.092 35
		PVP	0.059 80	0.054 15	0.008 62	0.089 79
		PSG	0.053 44	0.049 94	0.009 56	0.088 34

contain additional information. Having $w_{\text{LRG}} = 0$ simply means that a pure ELG power-spectrum is better at constraining the f parameter compared to any other mixture of ELGs and LRGs.

Fig. 3 shows the resulting variance of the four parameters for a variety of weights starting at (0.0, 1.0) – only ELGs – and going to (1.0, 0.0) – only LRGs – in steps of 0.1, as well the **FKP**, **PVP**, and **PSG** weighting schemes, in the first redshift bin for the DESI mocks. The points show the actual variance in measured parameter values from the mocks, while the lines show theoretical predictions based on our Fisher matrix formalism.

It is remarkable that the measured variances follow the theoretical predictions very closely. The fact that the minimums of the theoretical curves match well to the measured minimum variance values shows that the methods presented in Section 2 are sufficiently accurate and could, in principle, be applied to any parameter that needs to be constrained, so long as non-linear effects can be safely ignored.

For the remaining redshift bins of the DESI mocks and all redshift bins of the eBOSS mocks, we simply report the variance of each parameter for the **FKP**, **PVP**, and **PSG** weights. These results are summarized in Table 3. It can be seen that the **PSG** weights derived here essentially always produce smaller variances on their associated parameter. However, there are some cases in which the **PSG** weights produce the same or larger variances than the **FKP** or **PVP** weights. We find that in these cases, the theoretical variances have a broad minimum similar to what is seen for α_{\perp} and α_{\parallel} in Fig. 3. This means that we expect the gains in those cases to be minimal at best, and small fluctuations in the measured variance about its true value could lead to the **PSG** weights having a slightly higher variance than the other weighting schemes.

The improvements made, on the other hand, can be quite large. For example, in the second redshift bin for the DESI mocks, the **PSG** weights reduce the variance in f by ~ 36 per cent compared to the **PVP** weights. On average, the improvements for b and f are ~ 14 and ~ 10 per cent, respectively. Yet, α_{\parallel} and α_{\perp} seem to be insensitive to the weighting as long as the LRG weights are not very low.

5 CONCLUSIONS

We have presented a method of determining the relative weights that will result in the minimal variance of cosmological parameters measured from a joint power spectrum of multiple tracers. Tests on mock catalogues replicating eBOSS and DESI samples show that these weights will result in a 10–35 per cent decrease in the variance of the measured growth rate parameter compared to the commonly used weighting schemes. Our weighting scheme is different from the one presented in Hamaus, Seljak & Desjacques (2012) as it aims to find a single power spectrum (a most optimal mixture of the tracers) that is optimal for the cosmological constraints, while the weights in Hamaus et al. (2012) aim to split the tracers in two groups in a way that is most optimal for the RSD parameters. The decision about which weights to use will depend on what kind of analyses one has in mind. If the cosmological parameters will be measured from the joint power spectrum, then the **PSG** weights are optimal; if the tracers will be split in two groups with a full multitracer analysis to follow, then the Hamaus et al. (2012) can be used to determine the most optimal splitting.

Our derivation relies on several simplifying assumptions that are commonly adopted when deriving optimal weights. We assume that the galaxy field is perfectly Gaussian and calculate the variance of

the power-spectrum and its sensitivity to cosmological parameters using linear theory. Smith & Marian (2015, 2016) showed that by abandoning some of these assumptions for the density dependent weighting the performance of the weights can be improved by a further 20 per cent. We do not expect such a large improvement in our case since the theoretical predictions based on our simplified treatment eventually turn out to be very close to the actual results (see Fig. 3).

The optimal weights are, by definition, different for different cosmological parameters. Fortunately, it seems as though for the eBOSS and DESI samples, related parameters have similar optimal weights. In this case, ‘average’ optimal weights, that are nearly optimal for all parameters of interest, can be found. A more optimal solution would be to compute each cosmological parameter from its own ‘custom-weighted’ power-spectrum and find the covariance between them from the mock catalogues. Another option is to go one step beyond and find the optimal weights for the dark energy parameters that are derived from f , α_{\parallel} , and α_{\perp} .

A logical continuation of this work is to extend the formalism to samples with varying number density along the redshift shell. One could also try to incorporate it with the weights designed to optimize the measurements by accounting for the redshift evolution of the sample. We leave these matters to a future investigation.

ACKNOWLEDGEMENTS

LS is grateful for the support from SNSF grant SCOPES IZ73Z0 152581, GNSF grant FR/339/6-350/14, and NASA grant 12-EUCLID11-0004. This work was supported in part by DOE grant DEFG 03-99EP41093. NASA’s Astrophysics Data System Bibliographic Service and the arXiv e-print service were used for this work. Additionally, we wish to acknowledge GNUPLLOT, a free open-source plotting utility which was used to create all of our figures. We acknowledge the use of the LAMBDA, part of the High Energy Astrophysics Science Archive Center (HEASARC). HEASARC/LAMBDA is a service of the Astrophysics Science Division at the NASA Goddard Space Flight Center.

REFERENCES

Alcock C., Paczynski B., 1979, *Nature*, 281, 358
 Anderson L. et al., 2012, *MNRAS*, 427, 3435
 Ballinger W. E., Peacock J. A., Heavens A. F., 1996, *MNRAS*, 282, 877
 Beutler F. et al., 2011, *MNRAS*, 416, 3017
 Beutler F. et al., 2012, *MNRAS*, 423, 3430
 Beutler F. et al., 2014, *MNRAS*, 443, 1065
 Bianchi D., Gil-Marín H., Ruggeri R., Percival W. J., 2015, *MNRAS*, 453, L11
 Birdsall C. K., Fuss D., 1969, *J. Comput. Phys.*, 3, 494
 Blake C. et al., 2011, *MNRAS*, 415, 2876
 Blazek J., Seljak U., Vlah Z., Okumura T., 2014, *J. Cosmol. Astropart. Phys.*, 4, 001
 Coles P., Jones B., 1991, *MNRAS*, 248, 1

Dawson K. S. et al., 2016, *AJ*, 151, 44
 de la Torre S. et al., 2013, *A&A*, 557, A54
 de Putter R., Wagner C., Mena O., Verde L., Percival W. J., 2012, *J. Cosmol. Astropart. Phys.*, 4, 19
 DESI Collaboration, 2016, Science Final Design Report. US Department of Energy Office of Science. Available at: <http://desi.lbl.gov/tdr/>
 Eisenstein D. J., Seo H.-J., Sirko E., Spergel D. N., 2007, *ApJ*, 664, 675
 Feldman H. A., Kaiser N., Peacock J. A., 1994, *ApJ*, 426, 23 (FKP)
 Frigo M., Johnson S. G., 2005, *Proc. IEEE*, 93, 216
 Gil-Marín H., Noreña J., Verde L., Percival W. J., Wagner C., Manera M., Schneider D. P., 2015, *MNRAS*, 451, 5058
 Grieb J. N., Sánchez A. G., Salazar-Albornoz S., Dalla Vecchia C., 2016, *MNRAS*, 457, 1577
 Hamaus N., Seljak U., Desjacques V., 2012, *Phys. Rev. D*, 86, 103513
 Hamilton A. J. S., 1997, *MNRAS*, 289, 285
 Hastings W. K., 1970, *Biometrika*, 57, 97
 Kaiser N., 1987, *MNRAS*, 227, 1
 Kazin E. A., Sánchez A. G., Blanton M. R., 2012, *MNRAS*, 419, 3223
 Laureijs R. et al., 2011, preprint (arXiv:1110.3193)
 Levi M. et al., 2013, preprint (arXiv:1308.0847)
 Lewis A., Challinor A., Lasenby A., 2000, *ApJ*, 538, 473
 McDonald P., Seljak U., 2009, *J. Cosmol. Astropart. Phys.*, 10, 007
 Martínez V. J., Saar E., 2002, *Statistics of the Galaxy Distribution*. Chapman & Hall/CRC, Boca Raton, FL
 Mohammed I., Seljak U., 2014, *MNRAS*, 445, 3382
 Paz D. J., Sanchez A. G., 2015, *MNRAS*, 454, 4326
 Pearson D. W., Samushia L., 2016, *MNRAS*, 457, 993
 Peebles P. J. E., 1980, *The Large-scale Structure of the Universe*. Princeton Univ. Press, Princeton
 Percival W. J. et al., 2001, *MNRAS*, 327, 1297
 Percival W. J., Verde L., Peacock J. A., 2004, *MNRAS*, 347, 645 (PVP)
 Pope A. C., Szapudi I., 2008, *MNRAS*, 389, 766
 Reid B. A. et al., 2010, *MNRAS*, 404, 60
 Ross A. J. et al., 2012, *MNRAS*, 424, 564
 Ross A. J. et al., 2013, *MNRAS*, 428, 1116
 Ruggeri R., Percival W., Gil-Marín H., Zhu F., Zhao G., Wang Y., 2016, preprint (arXiv:1602.05195)
 Samushia L. et al., 2011, *MNRAS*, 410, 1993
 Schlegel D. J. et al., 2009, preprint (arXiv:0904.0468)
 Schlegel D. et al., 2011, preprint (arXiv:1106.1706)
 Schneider M. D., Cole S., Frenk C. S., Szapudi I., 2011, *ApJ*, 737, 11
 Scoccimarro R., 2015, *Phys. Rev. D*, 92, 083532
 Simpson F., Peacock J. A., 2010, *Phys. Rev. D*, 81, 043512
 Slepian Z., Eisenstein D. J., 2016, *MNRAS*, 455, L31
 Smith R. E., Marian L., 2015, *MNRAS*, 454, 1266
 Smith R. E., Marian L., 2016, *MNRAS*, 457, 4285
 Spergel D. et al., 2013, preprint (arXiv:1305.5422)
 Taruya A., Saito S., Nishimichi T., 2011, *Phys. Rev. D*, 83, 103527
 Tegmark M., Taylor A. N., Heavens A. F., 1997, *ApJ*, 480, 22
 Weinberg D. H., Cole S., 1992, *MNRAS*, 259, 652
 Xu X., Padmanabhan N., Eisenstein D. J., Mehta K. T., Cuesta A. J., 2012, *MNRAS*, 427, 2146
 Zhao G.-B. et al., 2016, *MNRAS*, 457, 2377
 Zhu F., Padmanabhan N., White M., 2015, *MNRAS*, 451, 236

This paper has been typeset from a \LaTeX file prepared by the author.